

Manuscript Number: NIMA-D-12-00776R1

Title: RF Strip-Line Anodes for Psec Large-Area MCP-based Photodetectors

Article Type: Research Paper

Section/Category: Gamma, X-ray and Charged Particle Detectors

Keywords: photodetector; anode; microstrip; stripline; microchannel plate; analog bandwidth; large-area detector

Corresponding Author: Prof. Henry Jonathan Frisch, Ph.D,

Corresponding Author's Institution: University of Chicago

First Author: Herve Grabas

Order of Authors: Herve Grabas; Henry Jonathan Frisch, Ph.D.; Eric Oberla; Jean-Francois Genat; Richard Northrop; David McGinnis; Bernhard Adams; Matthew Wetstein, Ph.D; Razib Obaid; Fukun Tang

Abstract: We have designed and tested economical large-area RF strip-line anodes made by silk-screening silver onto inexpensive plate glass, for use in microchannel plate photodetectors to provide measurements of time, position, integrated charge, and pulse waveform shapes. The 229-mm-long anodes are modular, and can be attached in series for economy in electronics channel-count. Measurements of the anode impedance, bandwidth and cross-talk due to inter-strip coupling are presented. The analog bandwidth, a key determinant of timing resolution, decreases from 1.6 GHz to 0.4 GHz as the anode length increases from 289 mm to 916 mm.

Dr. William A. Barletta
Editor
Nuclear Inst. and Methods in Physics Research, A
In re: Ms. Ref. No.: NIMA-D-12-00776
Title: RF Strip-Line Anodes for Psec Large-Area MCP-based Photodetectors
Nuclear Inst. and Methods in Physics Research, A

Dear Dr. Barletta,

We have resubmitted the above paper with the requested corrections. We'd like to thank the referee for a thoughtful and helpful set of comments. The paper is significantly improved due to the suggestions.

We apologize for the delay in getting this back- redoing the figures took time, and we ran a large DOE review of LAPPD plus the holidays.

Sincerely, Henry Frisch

1 RF Strip-Line Anodes for Psec Large-Area MCP-based
2 Photodetectors

3 Hervé Grabas^a, Razib Obaid^a, Eric Oberla^a, Henry Frisch^a, Jean-Francois
4 Genat^{a,1}, Richard Northrop^a, Fukun Tang^a, David McGinnis^b, Bernhard
5 Adams^c, Matthew Wetstein^{c,2}

6 ^a*Enrico Fermi Institute, University of Chicago*

7 ^b*European Spallation Source, Lund, Sweden*

8 ^c*Argonne National Laboratory*

9 **Abstract**

We have designed and tested economical large-area RF strip-line anodes made by silk-screening silver onto inexpensive plate glass, for use in microchannel plate photodetectors to provide measurements of time, position, integrated charge, and pulse waveform shapes. The 229-mm-long anodes are modular, and can be attached in series for economy in electronics channel-count. Measurements of the anode impedance, bandwidth and cross-talk due to inter-strip coupling are presented. The analog bandwidth, a key determinant of timing resolution, decreases from 1.6 GHz to 0.4 GHz as the anode length increases from 289 mm to 916 mm.

¹Present address, LPNHE, CNRS/IN2P3, Universités Pierre et Marie Curie and Denis Diderot, T33 RC, 4 Place Jussieu 75252 Paris CEDEX 05, France

²Joint Appointment with the Enrico Fermi Institute, University of Chicago

10 **1. Introduction**

11 The development of large-area (m^2) photodetectors with time resolutions
12 of picoseconds (10^{-12} sec) and sub-millimeter space resolutions would open
13 new opportunities in many areas, including collider detectors, rare kaon ex-
14 periments, and neutrino experiments in particle and nuclear physics, X-ray
15 detection at light sources, and Time-of-Flight Positron Emission Tomography
16 (TOF-PET) [1, 2]. Micro-Channel Plate Photomultipliers (MCP-PMTs) [3]
17 have previously been shown to provide space resolutions of a few microns [4],
18 time resolutions down to 5 psec [5], and risetimes as short as 60 psec [6]. MCP-
19 based detectors with bandwidths in the GHz regime are predicted to give sub-
20 psec time resolutions [2, 7].

21 Capacitively-coupled anodes have been developed with good space and time
22 resolutions for a number of applications [8–11]. In this paper we describe the de-
23 sign and testing of economical strip-line anodes [12] with RF analog bandwidths
24 in the GHz range and lengths up to 92 cm being developed by the LAPPD Col-
25 laboration [13] for large-area MCP-based photodetectors. The design described
26 here was set at a point in the parameter space of cost, time resolution, space
27 resolution, area covered per channel, and channel density, appropriate for appli-
28 cations requiring large area, low cost, and modest resolutions (<10 psec in time
29 and 400 microns in space for signals from charged particles and high-energy
30 photons, and <100 psec and 2 mm for single visible photons). A different op-
31 timization of the design would allow the construction of higher performance
32 anodes for applications that require better resolution [14].

33 The LAPPD design is based on an MCP consisting of a $20 \times 20 \text{ cm}^2$ ($8'' \times 8''$)
34 capillary glass plate with $20\text{-}\mu\text{m}$ pores [15], functionalized with resistive and
35 emissive layers using Atomic Layer Deposition [16–19]. This method allows
36 separately optimizing the three functions performed by a conventionally con-
37 structed MCP: providing the pore structure, a resistive layer for current supply,
38 and the secondary emitting layer. In addition, the micro-pore substrates are a
39 hard glass, providing a more chemically stable platform and improved mechan-

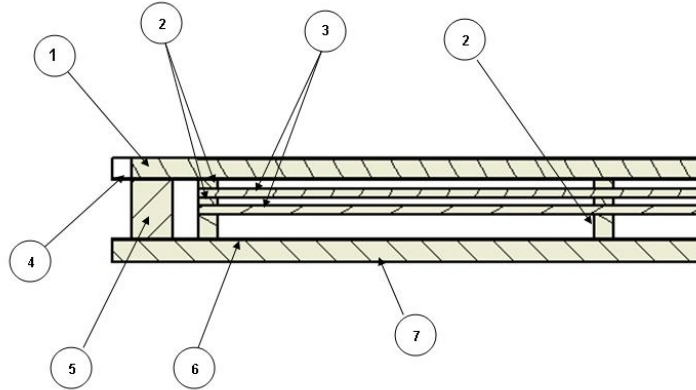
40 ical strength.

41 The structure of the LAPPD MCP-PMT vacuum photodetector is shown
42 in Figure 1 [13]. A photo-cathode is deposited on the vacuum side of the top
43 window, which is followed by an accelerating gap for the initial photo-electron, a
44 pair of 20×20 cm² MCPs in a chevron geometry that amplify the single electron
45 by a factors up to 5×10^7 , a gap after the output of the second MCP, and an
46 anode plane that collects the amplified pulse of electrons. Incident photons are
47 converted into electrons by the photo-cathode. Each of these photo-electrons
48 is accelerated into a pore of the micro-channel plate where it causes a cascade
49 by the process of secondary emission. The electrons emerging from the far ends
50 of the pores are then accelerated towards an anode where they are collected.
51 Measuring the time and position of the anode pulse gives both time and space
52 resolution information on the incoming particle [8–11]. The intrinsic granularity
53 is set by the pores; there are approximately 80 million pores in one of the 8”
54 20-micron pore Incom glass substrates in the baseline LAPPD design [15]. The
55 granularity of the readout is set by the anode pattern, which is quite flexible,
56 allowing many possible patterns and channel sizes [20].

57 *1.1. Picosecond timing measurement and spatial resolution*

58 Due to the small feature size of the amplification stage, MCP-based photode-
59 tectors are intrinsically very fast, with risetimes measured down to 60 psec [6].
60 MCP’s are also spatially homogeneous, so that the risetimes are equally fast
61 everywhere on the photodetector area. An essential step in developing fast
62 photodetector systems with areas measured in meters-squared is thus the de-
63 velopment of a large-area inexpensive anode with an analog bandwidth capable
64 of retaining the intrinsic speed of the pulse. Parametric extrapolations with
65 higher system analog bandwidth, using sampling rates and signal-to-noise ra-
66 tios already achieved, predict time resolutions well below 1 psec [7].

67 The potential exists for even faster MCP risetimes by using smaller pore sizes
68 enabled by the stronger glass of the borosilicate substrate, higher secondary
69 emission yield (SEY) materials at the top of the pores, and ALD-based discrete



- | | |
|--|------------------------------------|
| 1. Top window with photocathode on inside | 5. Side wall |
| 2. Grid spacers | 6. Anode transmission lines |
| 3. Microchannel plates | 7. Bottom window |
| 4. HV contact | |

Figure 1: The basic structure of the glass LAPPD MCP-PMT detector. The sealed vacuum tube consists of a top window with the photocathode on the inner surface, an accelerating gap for the initial photo-electron, a pair of 20-cm-square MCPs in a chevron geometry that amplify the photo-electron by factors up to 5×10^7 , a gap after the output of the second MCP, and the anode that collects the exiting ‘cloud’ of electrons. The package is less than 15 mm thick.

70 dynode structures inside the pores [21].

71 Spatial resolution depends as well on the small feature size of the MCP pores,
 72 which provide an intrinsic resolution on the order of the size of the pore. Mea-
 73 surements with spatial resolutions down to 5 microns have been reported using
 74 strip-line anodes [4]. The RF-stripline anode design presented here, however,
 75 is focused on applications where excellent time resolution is needed over large
 76 areas.

77 1.2. Outline

78 A brief outline of the paper as a guide to the reader follows. The calculation
 79 of time and position using the time-of-arrival of the pulses at both ends of the

80 strips of the transmission line anode is presented in Section 2. Section 3 describes
81 the anode construction of inexpensive plate glass and silk-screened silver strips.
82 The techniques and test setups used to make the measurements of bandwidth,
83 impedance, attenuation, and cross-talk in the frequency domain are described in
84 Section 4. Sections 5, 6, and 7 present measurements and predictions of anode
85 impedance; bandwidth; and attenuation and crosstalk, respectively. Section 8
86 summarizes the conclusions.

87 **2. Using RF Strip-line anodes and wave-form sampling to measure** 88 **position, time, and properties of the pulses**

89 The charge cloud of the electrons emerging from the pores of the MCP stack
90 holds both the space and time information generated by the initial photon or
91 relativistic charged particle impinging on and traversing the window [22]. In
92 the LAPPD design, shown in Figure 1, the charge cloud propagates towards
93 an array of multiple strip-lines. On each strip-line, the pulses created by the
94 charge excitation propagate in opposite directions to the ends of the line, where
95 they are digitized by waveform sampling. From the digitized pulses at each
96 end one can determine the time, position, total charge, and pulse shape of the
97 impinging particles. The spatial location of the charge along the strip direction
98 is determined from the difference in times measured on the two ends of a strip.
99 The one-dimensional nature preserves the excellent space resolution but with
100 many fewer channels of electronics than with a two-dimensional pixel array. In
101 the transverse direction the resolution is determined by the strip spacing in
102 the present 1-dimensional implementation of the anode [23]. The time of the
103 deposited charge is given by the average of the times at the two ends of the
104 strip.

105 The precision of both time and space measurements depends on four param-
106 eters of the pulses that arrive at the end of a strip [2, 7]: 1) the signal-to-noise
107 ratio; 2) the risetime of the pulse; 3) the sampling frequency of the digitization;
108 and 4) fluctuations in the signal itself. The risetime of the detected pulse will be

109 limited by the analog bandwidth of the strip-line for applications with low-cost
 110 large-area readout [2, 20]. It is the analog bandwidth of the strip-lines that is
 111 the focus of this paper.

112 The glass package design uses the MCP internal components for both the
 113 DC HV current supply and the fast signal generation. In particular, the anode
 114 plane of RF strip-lines provides both the signal virtual ground and the HV DC
 115 ground, as shown in Figure 2. Multiple tiles can be daisy-chained by bridging
 116 the strip-lines on one tile to the next, forming a continuous strip-line. Each
 117 strip-line is terminated in 50Ω at each end of a tile-row, where the read-out
 118 electronics is located.

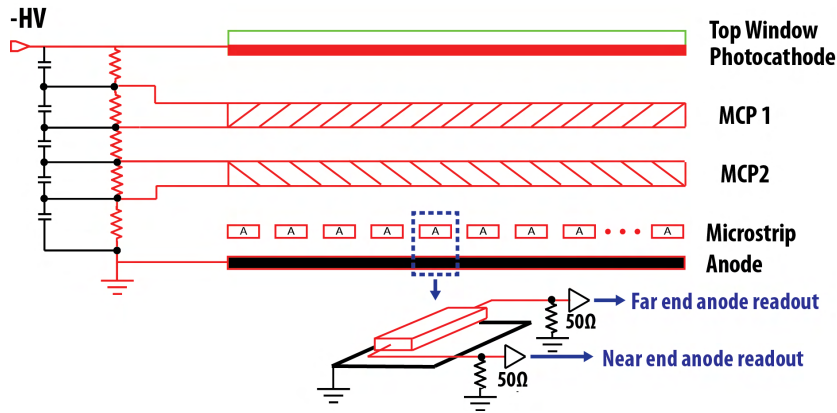


Figure 2: The equivalent electrical HV and signal circuits of the strip-line anode. The silver strip-lines are fired onto the top surface of the glass plate that forms the bottom of the tile package. The sealed tiles (See Figure 1) sit on a copper sheet, which acts as the ground plane for the strip-line. Each strip-line is terminated in 50Ω at each end.

119 The time-of-arrival information at each end of a strip is extracted from the
 120 leading edge, the peak, and a portion of the trailing edge of the pulse just
 121 beyond the peak, at each end of the strip [2]. The measurement of relative
 122 times-of-arrival at the two ends benefits from the inherent correlation between
 123 the shapes of the pulses at each end of the strip. Using a commercial MCP

124 excited by a laser as a source, we have measured a relative resolution of 2 psec
125 on a 5"-ceramic-substrate strip-line anode [24]. Using a pair of the LAPPD 8"
126 MCPs [25] and a 229-mm-long 30-strip glass anode (see the left-hand panel of
127 Figure 3), we have measured a relative resolution of <5 psec [25].

128 The difference in times-of-arrival between the pulses recorded at the two
129 ends of the strips provides a measurement of the position of the incident radi-
130 ation in the direction along the strips. The anodes used here have a nominal
131 impedance of 50Ω and a measured propagation velocity of $0.57\pm 0.07 c$ ($170\pm$
132 20 microns/psec). The correspondence between the position resolution δx and
133 the time resolution of the pulse δt is given by $\delta x \approx 1/2 \delta t \times v$, where v is the
134 propagation velocity.

135 The position in the direction transverse to the strips is measured by simul-
136 taneously digitizing the signals on every strip in the 1-dimensional anode design
137 presented here. The strip or strips closest to the position of the incident radi-
138 ation will carry the largest signal. The neighboring strips carry signals induced
139 capacitively and inductively (see Section 7). While energy is transferred from
140 the central strip into the neighboring strips, not all information is lost, as the
141 neighboring strips are digitized. In the ideal limit of zero noise the information
142 can be completely recovered in the case of a single hit.

143 A benefit of the wave-form digitization readout is that it gives the equivalent
144 of an oscilloscope trace for both ends of each of the strip-lines, allowing the
145 extraction of amplitude, integrated charge, shape, and separation of overlapping
146 or near-by pulses ('pile-up') [2]. The measured shape will depend on the analog
147 bandwidth, cross-talk, attenuation, and signal-to-noise ratio of the system, and
148 will thus depend on the position of the incident excitation for large systems.
149 In addition, care has to be taken in impedance matching the detector to the
150 electronics to avoid losses from reflections at interfaces.

151 Reference [2] contains a comparison of methods to extract the time-of-arrival
152 of a pulse. A study of the benefit of using a more sophisticated fit to the pulse
153 shape is presented in Ref. [26]. Waveform sampling allows extracting much
154 more information than just the time, however; a fit to a template shape allows

155 the extraction of the amplitude, integrated charge, a figure-of-merit for the
156 goodness of fit to the shape, and possible separation of nearby or overlapping
157 pulses. Algorithms such as these can be implemented in FPGA-based processors
158 located close to the waveform digitization front-end, allowing only the higher-
159 level parameters of the pulse to be transmitted to the next level of analysis [27].

160 **3. Anode Design and Construction**

161 The aim of the LAPPD project is to develop a large-area economical pho-
162 todetector with good space and time resolution, low electronics channel count
163 and power, and low noise. We have developed a mechanical design based on
164 inexpensive commercial float glass [28]. This glass can be water-jet cut, and so
165 many aspects of the construction are widely available and standard in industry.
166 In this section we describe the application of these principles to the design and
167 construction of the anode.

168 *3.1. Choice in Anode Parameter Space for the Proof-of-Concept Detector*

169 The LAPPD project was started in 2009 with the goal of developing a com-
170 mercializable module in three years. Choices had to be made for the initial pa-
171 rameters for proof-of-concept, with the understanding that after the three-year
172 R&D phase, modules for specific applications would be designed with optimized
173 parameters. The parameters of the initial design described here were chosen to
174 be appropriate for applications requiring large area, low cost, and modest res-
175 olutions. The flexibility of the design, however, should allow optimizations for
176 very precise timing at colliders and other applications.

177 The initial choice of an 8"-square (200 mm) module was made to be signifi-
178 cantly larger than available MCP-PMT's but sized to widely-available vacuum
179 components and light enough to be handled by vacuum transfer equipment. In
180 addition, a 200-mm anode is long enough to be treated as a transmission line
181 for typical MCP risetimes.

182 The glass package as well as the anode glass substrate were chosen for cost
183 considerations - Borofloat glass [28] is widely available and inexpensive. Evap-
184 oration and sputtering to form the metalized strip-lines on the surface of the
185 anode were successfully tried; however the silk-screening of silver-loaded ink [29]
186 proved significantly less expensive with a very fast turnaround, as a silk-screen
187 is much more easily produced than a mask, and the silk-screening process is
188 entirely mechanized and in air rather than in vacuum. The high-frequency be-
189 havior of the glass and silk-screened silver are adequate to handle the bandwidth
190 of the present generation of 20-micron pore MCP's.

191 The choice of the anode strip width was set by a choice of a 50Ω strip
192 impedance. This is determined by the thickness of the glass anode substrate
193 (2.75 mm) and the dielectric constant of the glass [28].

194 The choice of the gap spacing between the anode strips depends on com-
195 peting considerations. The crosstalk between strips decreases with gap size.
196 However a large gap provides a high-resistance area on which charge could ac-
197 cumulate, possibly leading to hysteresis or breakdown at high rates. A larger
198 gap size diminishes the electronics channel count but increases the transverse
199 spatial resolution [23].

200 *3.2. The Single Tile Anode*

201 The LAPPD design is modular, with the unit module being a sealed planar
202 glass vacuum tube with an 8" (200 mm)-square active area, called a 'tile'. The
203 metal strips that form the anode for the tile are formed by the inexpensive
204 technique of silk-screening a silver-based ink [29] onto the glass plate, and then
205 firing the plate at high temperature [30] to burn off the volatiles, leaving behind
206 the silver traces. The thickness of the silver trace is typically 10-15 μm . The
207 dimensions of the glass plate, 229.1 mm by 220.0 mm, are set by the design of the
208 8"-square MCP-PMT active area. A single tile is shown in the left-hand panel
209 of Figure 3; the 'fanout' cards used for measurements with the pulse generator,
210 oscilloscope, and network analyzer are shown in the right-hand panel.

211 Two anode strip patterns have been tested, one with 30 strips and the other

212 with 40, both with a 50Ω target impedance. The 40-strip anode was an initial
213 design, with small gaps between the strips designed to minimize possible static
214 electric charging of the inter-strip glass, and was well-matched to then-current
215 waveform sampling PSEC-3 ASIC which had 4 channels, requiring 10 chips per
216 end [31]. The 30-strip anode is matched to a new 6-channel PSEC-4 ASIC [27],
217 halving the chip count to 5 chips per end. The strip width, strip gap, and
218 plate thickness of the 30-strip anode are 4.62 mm, 2.29 mm, and 2.75 mm,
219 respectively. The corresponding numbers for the 40-strip anode are 3.76 mm,
220 1.32 mm, and 2.67 mm.

221 3.3. The Multi-Tile Anode

222 The strip lines of one tile can be connected in series with the strip lines of a
223 neighboring tile to make a ‘tile-row’ that shares the common readout on the two
224 ends of the shared multi-tile strip, as shown for a 3-tile tile-row in Figure 4. The
225 strips on the connected tiles form continuous 50Ω transmission lines with the
226 ground plane that underlies all the tiles. At each end of a tile-row a fanout card
227 makes the transition to SMA connectors for each strip. Each strip is terminated
228 in 50Ω , either at the oscilloscope, or, if the SMA connector is left open, with a
229 50Ω resistor at the connector.

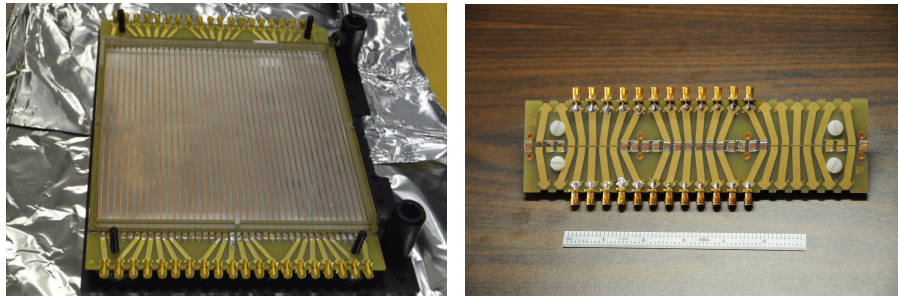


Figure 3: Left: A single tile with a 229.1 mm-long 40-strip anode. The anode strips are connected at both ends to the fanout cards used for testing. Right: A ‘zero-length tile’ consisting of a pair of fanout cards, used to characterize the measurement system with no tile.

230 Measurements were made with anodes consisting of 1, 3, and 4 tiles, where
231 each tile anode is 229.1 mm-long. In addition, measurements were made with
232 a 115 mm-long ‘half-tile’, and, in order to unfold the contribution of the test
233 setup cabling and fanout cards, with the zero-tile configuration, as shown in
234 the right-hand panel of Figure 3. The connections between anodes are made
235 by hand-soldering small strips of copper to the silver silk-screened strips on the
236 glass, as shown in Figure 4.

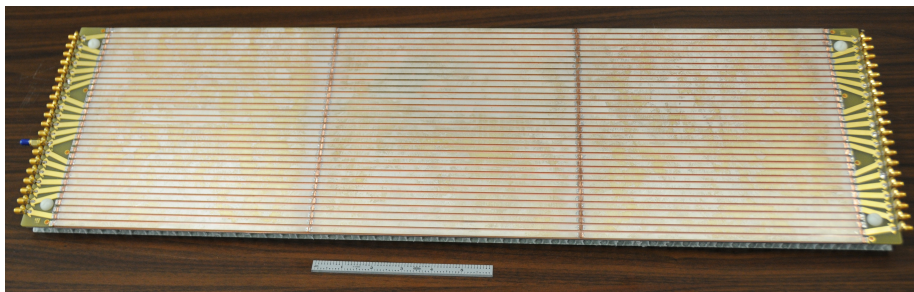


Figure 4: The 3-tile anode used to measure bandwidth, attenuation, and impedance as a function of anode strip length. The connections between anode strips on neighboring tiles have been made by soldering small strips of copper to the silver silk-screened strips on the glass.

237 4. Anode Performance

238 To characterize the bandwidth, attenuation, cross-talk, and impedance of
239 the anodes, signals are introduced via SMA cables to the fanout card at one
240 end of one strip (the ‘active’ strip), and measurements are made at the far and
241 near ends of that strip and neighbors (‘quiet’ strips). We describe the details
242 below.

243 4.1. Impedance Matching to the Strips

244 The transition of the \vec{E} and \vec{B} fields between the geometries of the coaxial
245 cable, the SMA cable, and the planar transmission line results in reflections and
246 signal distortion. This can be handled by designing a transition region to match

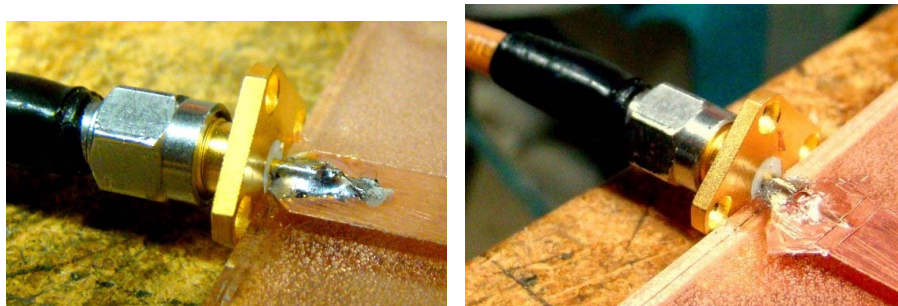


Figure 5: The geometry of the coupling between the coaxial cable from the pulse generator to the anode strip before modification (Left), and after impedance matching with copper tape (Right).

247 the impedances. Rather than using a full wave simulator to get a theoretical
248 solution, we used an empirical method of tuning by hand while watching the
249 match with a network analyzer. We used adhesive-backed copper tape [32]
250 to construct geometries on the glass substrate. Monitoring the work in the
251 time domain on a network analyzer, one can identify the location of impedance
252 mismatches and make appropriate additions (more capacitance) or subtractions
253 (more inductance) of metal. After optimization, a single shape was adequate
254 for all the strips in the 30-strip tile, as expected.

255 The left-hand panel of Figure 5 shows the geometry of the coupling between
256 the coaxial cable from the pulse generator to the anode strip before modification,
257 and on the right, after correction.

258 *4.2. Measurements of Pulse Rise Times*

259 The anode responses to a step-function with a risetime of 200 psec introduced
260 into one end of a strip in a multi-strip anode were measured using the reference
261 fast edge of the calibration output from a Tektronix TDS6154C oscilloscope, as
262 shown in Figure 6. The 30-strip anode has better bandwidth performance than
263 the 40-strip due to less coupling to neighboring strips. The length of the anode
264 also enters into performance, as the energy transfer to neighboring strips grows
265 with strip length.

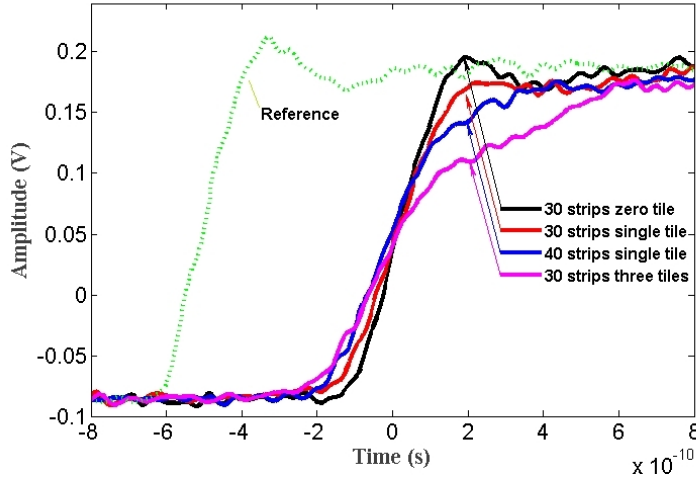


Figure 6: The anode responses in the time domain to a step-function introduced into one end of a strip in a multi-strip anode. The source of the reference pulse is the calibration output from a Tektronix TDS6154C oscilloscope, which has a risetime of 200 psec and an amplitude of 440 mV (peak-peak). The response curves in the figure were measured with the same oscilloscope.

266 *4.3. Measuring the Bandwidth, Attenuation, Velocity, and Impedance*

267 Measurements of analog bandwidth, attenuation, propagation velocity, cross-
 268 talk, impedance, and RF matching were made with an Agilent HP8753E network
 269 analyzer [33]. For each tile configuration, signals were introduced from one port
 270 on one end of an anode strip via a fanout card, and measured at the far end via
 271 a second fanout card. The power on both the near end and the far end were
 272 recorded as a function of frequency. The signals on both ends of neighboring
 273 strips were also recorded. The results are given in Sections 5, 6, and 7 below.

274 **5. Impedance**

275 The impedance of a single strip of width w separated from an infinite ground
 276 plane by a glass substrate of thickness h depends on the ratio of strip width to
 277 strip-ground plane separation, w/h [34].

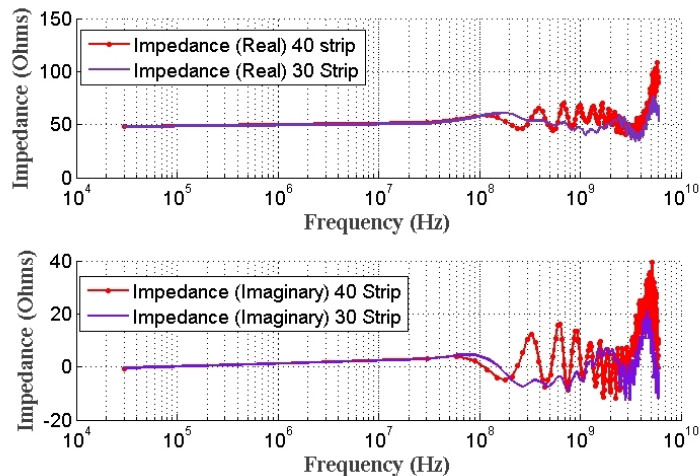


Figure 7: The measured real (top) and imaginary (bottom) impedance versus frequency for 40-strip and 30-strip silk-screened anodes on a single 229.1 mm-long glass tile base between two fanout cards. The targeted design impedance (top) was 50Ω .

278 In the case of an array of multiple strip-lines, the impedance of the lines is
 279 more complicated, as the geometry of the field lines is affected by the adjacent
 280 strips. Consequently additional excitation (odd and even) modes exist, modify-
 281 ing the impedance of the single strip-line mode [35–37]. The impedance of the
 282 lines is thus not only a function of the w/h ratio but also of the width of the
 283 gap between the strips.

284 Figure 7 shows the measured real and imaginary parts of the impedance ver-
 285 sus frequency for 40-strip and 30-strip silk-screened anodes on a single 229.1 mm-
 286 long glass tile base between the fanout cards. The targeted design impedance
 287 (real part) was 50Ω . The impedances are well-matched to the few-GHz band-
 288 width of the present MCP’s. The imaginary part of the 30-strip anode stays
 289 relatively small up to the few-GHz region, well-matched to the bandwidth of
 290 the present LAPPD 220-mm-square 20-micron pore MCP’s.

291 **6. Bandwidth**

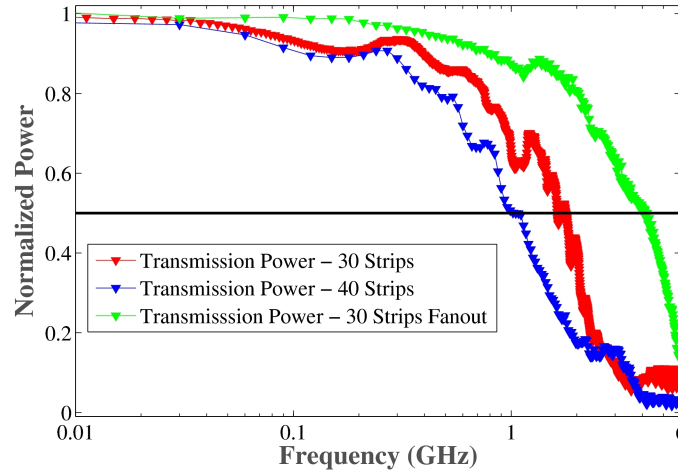


Figure 8: The normalized power (output power/input power) versus log-frequency for a single 229.1 mm-tile plus fanout cards(288.5 mm) with 30 strips (red, middle trace), 40 strips (blue, bottom trace), and the fanout PC cards alone(‘zero-tile’, in green, top trace). See Figure 3. The (black) horizontal line represents the 3db loss level (50% loss in power).

292 In a strip-line anode geometry, a wave traveling on one strip will also transfer
 293 energy to its neighbors due to inductive and capacitive coupling between the
 294 strip-lines [36, 37]. We have measured the bandwidth over different length strip-
 295 lines by connecting the 229.1 mm anode of the tile to a neighboring tile or tiles
 296 in series, as shown in Figure 4.

297 Figure 8 shows the measured ratio of output power to input power versus
 298 frequency for the three cases of a single 30-strip anode with fanout cards, a
 299 single 40-strip anode with fanout cards, and just the fanout cards alone (‘zero-
 300 tile’). The 30-strip tile has significantly improved analog bandwidth, as well
 301 as providing the reduced channel count for the 6-channel PSEC-4 ASIC. No
 302 correction has been made for the fanout cards, as they have significantly higher
 303 bandwidth than the anodes.

304 Figure 9 shows the measured 3-dB loss point in frequency for different length
 305 anodes. The points shown correspond to the effective length of the fanout card
 306 pair alone (59.4 mm), a single tile with fanout cards (288.5 mm), and, in the
 307 case of the 30-strip anode, three and four tiles with fanout cards (746.7 mm and
 308 916 mm, respectively). The slope of the exponential fit of the bandwidth (GHz)
 309 versus the log of the length in cm is -3.19.

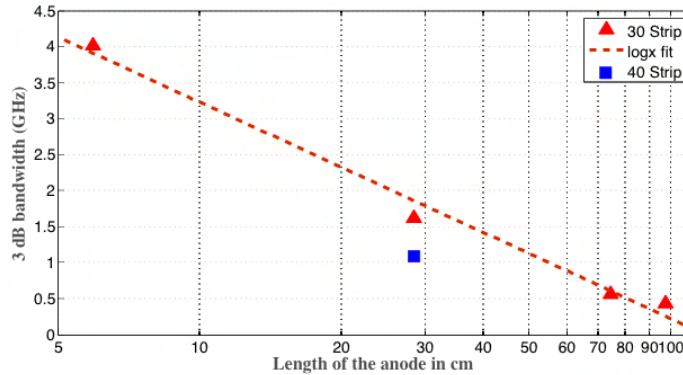


Figure 9: The bandwidth measured at 3dB loss on the central strip versus the log of the total anode length. The anodes consisted of 3 and 4 tiles in series (746.7 mm and 916 mm, respectively, including the length of the fanout card strips), a single tile (288.5 mm), and only the 2 fanout PC cards connected to each other ('zero tiles'- 59.4 mm).

310 7. Attenuation and Cross-talk

311 The power in a pulse propagating down a strip diminishes with distance
 312 due to resistive attenuation in the materials of the strip and coupling to neigh-
 313 boring strips. Two adjacent strip-lines are both capacitively and inductively
 314 coupled [35]. A wave traveling down the line induces a signal on its neighbors.
 315 This cross-talk, which is the dominant source of loss at high frequencies, pro-
 316 duces pulses both at the near and far end of the adjacent strips, as shown in
 317 Figure 10. The degree of acceptable energy loss and signal mixing from one strip
 318 to another is application-specific, and can be optimized by changing the strip

319 spacing and impedance, or by using a material with an appropriate dielectric
 320 constant.

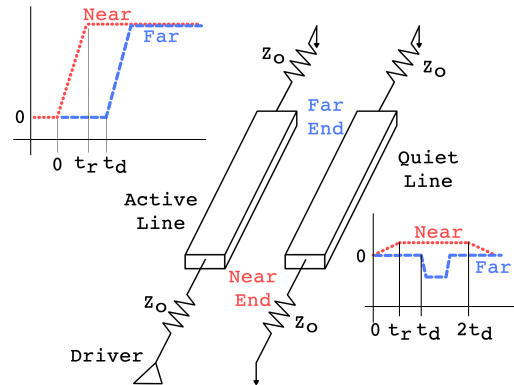


Figure 10: The mechanism of cross-talk for a positive signal with a linear rising edge [35]. Two adjacent strip-lines are shown; the common ground plane is not shown for clarity. The active line is driven on the near end with a signal pulse of rise-time t_r . At the far end of the active line the same pulse is seen a time t_d later, determined by the length and characteristic velocity of the line. The neighboring line, the quiet line, is coupled to the active line capacitively and inductively by the electric and magnetic fields, respectively. At the near end of the quiet line a positive voltage appears at the start of the signal and persists for $2t_d$. For an inductive coupling, at the far end a negative voltage appears starting at t_d with a width t_r .

321 Figure 11 shows measurements of the normalized power measured in the
 322 driven strip (Strip 0) and neighboring strips. A signal is input on the central
 323 strip (shown in red) via the fanout card and is detected at the far end. The
 324 power is measured on the near and far ends of the strips. The left-hand plot
 325 shows the sum of the two ends for each strip. A single 30-strip tile is shown as
 326 triangles; measurements on an anode made of three 30-strip tiles in series (see
 327 Figure 4) are represented by squares. A single 40-strip tile is shown as circles.

328 The single 30-strip tile has the lowest cross-talk, as expected due to its wider

329 spacing than the 40-strip tile, and shorter length than the anode composed of
 330 three 30-strip tiles. The effect of cross-talk on pattern recognition will depend
 331 on the specific application (specifically occupancy and signal-to-noise), and the
 332 implementation of digitization and pattern-recognition algorithms.

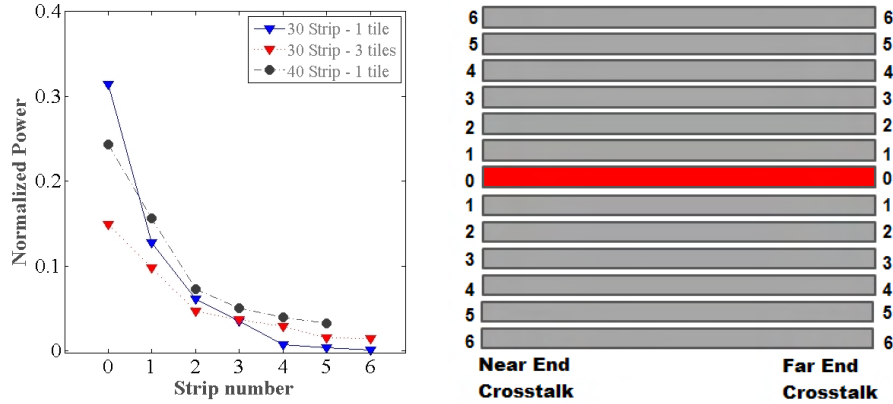


Figure 11: Comparison of total normalized power summed over all strip-lines for three different anode geometries: a single 30-strip tile (triangles), a single 40-strip tile (circles), and three 30-strip tiles in series. The right-hand panel shows the geometry of the test setup: A signal is input on the near end of the central strip (shown in red) and is detected at the far end. The power is measured on the near and far ends of the neighboring strips.

333 8. Conclusions

334 Anodes for MCP-PMT's with analog bandwidths in the GHz region are pre-
 335 dicted to enable sub-psec time resolutions for applications that provide enough
 336 initial signal. We have measured the signal properties of a class of inexpen-
 337 sive anodes for use in large-area microchannel plate detectors and other current
 338 sources. The strip-line anodes are inexpensively constructed by silk-screening
 339 silver ink on widely-available borosilicate float glass. The unit 'tile' anode is
 340 229-mm long; the units can be daisy-chained in series to cover more area with
 341 the same electronics channel count. The present LAPPD glass-based design

342 uses 30 anode strips to cover the 220-mm wide anode.

343 We measure an analog bandwidth of 1.6 GHz on a single tile, and present
344 the bandwidth as a function of the number of tiles for anode strip lines up to
345 916 mm in length. Results on attenuation, cross-talk, impedance, and signal
346 velocity are also presented. We also describe the techniques and equipment used
347 in the measurements.

348 **9. Acknowledgments**

349 We thank our colleagues in the Large Area Psec Photodetector (LAPPD)
350 Collaboration for their contributions and support. Particular thanks are due to
351 M. Heintz for critical technical support, G. Varner for RF advice, and R. Metz
352 and M. Zaskowski for machining and mechanical work. J. Gregar (ANL), P.
353 Jaynes (CatI Glass), and E. A. Axtell (Ferro Corporation) provided invaluable
354 advice and technical support on the glass and silver anode application tech-
355 niques.

356 The activities at Argonne National Laboratory were supported by the U.
357 S. Department of Energy, Office of Science, Office of Basic Energy Sciences
358 and Office of High Energy Physics under contract DE-AC02-06CH11357, and
359 at the University of Chicago by the National Science Foundation under grant
360 PHY-1066014.

361 **References**

- 362 [1] T. Credo (IMSA), H. Frisch, H. Sanders, R. Schroll, and F. Tang, *Picosec-*
363 *ond Time-of-Flight Measurement for Colliders Using Cherenkov Light*, Pro-
364 ceedings of the IEEE, Rome, Italy, Oct. 2004; Nuclear Science Symposium
365 Conference Record, 2004 IEEE, Volume: 1 Date: 16-22 Oct. 2004.
- 366 [2] J.-F. Genat, G. S. Varner, F. Tang, H. Frisch, *Signal Processing for Pico-*
367 *second Resolution Timing Measurements*, Nucl. Instrum. Methods A 607
368 (2009) 387; arXiv:0810.5590.

- 369 [3] J.L. Wiza, *Micro-channel Plate Detectors*, Nucl. Instrum. Methods 162
370 (1979) 587.
- 371 [4] A.S. Tremsin and O.H.W. Siegmund, *Charge cloud asymmetry in detectors*
372 *with biased MCPs*, Proceedings SPIE3 4497 (San Diego, California) (2001).
373 A parallel LAPPD effort with a different anode technology, based at the
374 Space Sciences Laboratory, UC Berkeley, is better suited to applications
375 needing high space resolution.
- 376 [5] K. Inami, N. Kishimoto, Y. Enari, M. Nagamine, and T. Ohshima, Nucl.
377 Instrum. Methods A560 (2006) 303.
- 378 [6] J. Milnes and J. Howorth (Photek Ltd.), *Advances in Time Re-*
379 *sponse Characteristics of Micro-channel Plate PMT Detectors*. See
380 http://www.photek.com/support/technical_papers.htm.
- 381 [7] S. Ritt, *The Factors that Limit Time Resolution in Photodetectors*,
382 Workshop, Univ. of Chicago, Chicago, IL, 28-29 April 2011. See
383 <http://psec.uchicago.edu/workshops/>. Note that of the values needed of
384 the four parameters to achieve a time resolution of 100 fsec (the bottom
385 row of the table of extrapolations), we have achieved or exceeded three:
386 sampling rate, noise, and signal size. Only the analog bandwidth falls short
387 at present.
- 388 [8] M. Lampton, *Delay line anodes for microchannel plate spectrometers*, Rev.
389 Sci. Instr. 58 (12) (1987) 2298.
- 390 [9] O.H.W. Siegmund: *Amplifying and position sensitive detectors, Methods*
391 *of vacuum ultraviolet physics*, Chapter III, 2nd edition, editors: J.A.R.
392 Sampson and D. L. Ederer, Academic Press, (1998).
- 393 [10] O. Jagutzki et al., *Multiple Hit Readout of a Microchannel Plate Detector*
394 *With a Three-Layer Delay-Line Anode*, IEEE Trans. Nucl. Sci. 49 (5) (2002)
395 2477.

- 396 [11] J.S. Lapington, J.R. Howorth, J.S. Milnes, *Demountable readout technolo-*
397 *gies for optical image intensifiers*, Nucl. Instrum. Methods A 573 (2007)
398 243.
- 399 [12] The LAPPD geometry of a strip over a ground plane is often called a
400 microstrip transmission line.
- 401 [13] The original LAPPD institutions include ANL, Arradance Inc., the
402 Univ. of Chicago, Fermilab, the Univ. of Hawaii, Muons, Inc., SLAC,
403 SSL/UCB, and Synkera Corporation. More detail can be found at
404 <http://psec.uchicago.edu/>.
- 405 [14] For a discussion of the factors that determine time and space resolution
406 in MCP-based detectors, see the talks at: *The Factors that Limit Time*
407 *Resolution in Photodetectors*, Workshop, Univ. of Chicago, Chicago, IL,
408 28-29 April 2011. See <http://psec.uchicago.edu/workshops/>.
- 409 [15] The glass capillary substrates are produced by Incom Inc., Charlton, Mass.
410 See <http://www.incomusa.com/>.
- 411 [16] S. M. George, *Atomic Layer Deposition: An Overview*, Chemical Reviews
412 110 (1) (2010) 111-131.
- 413 [17] J. W. Elam, D. Routkevitch, and S. M. George, *Properties of ZnO/Al₂O₃*
414 *Alloy Films Grown Using Atomic Layer Deposition Techniques*, Journal of
415 the Electrochemical Society 150 (6) (2003) G339-G347.
- 416 [18] D. R. Beaulieu, D. Gorelikov, H. Klotzsch, P. de Rouffignac, K. Saadat-
417 mand, K. Stenton, N. Sullivan, and A. S. Tremsin, *Plastic microchannel*
418 *plates with nano-engineered films*, Nucl. Instrum. Methods A 633 (2011)
419 S59-S61.
- 420 [19] O.H.W. Siegmund, J.B. McPhate, S.R. Jelinsky, J.V. Vallerga, A.S. Trem-
421 sin, R. Hemphill, H.J. Frisch, R.G. Wagner, J. Elam, and A. Mane, *Devel-*
422 *opment of Large Area Photon Counting Detectors Optimized for Cherenkov*

- 423 *Light Imaging with High Temporal and sub-mm Spatial Resolution*, Pro-
424 ceedings IEEE NSS-MIC, Valencia Spain (2011).
- 425 [20] *Large Area, Pico-second Resolution, Time of Flight Detectors*;
426 US Patent US 2007/0187596 A1; Aug 16, 2007; Inventors: H. J. Frisch, H.
427 Sanders, F. Tang, T. Credo.
- 428 [21] J.W. Elam, J. A. Libera, M.J. Pellin, and P.C. Stair, *Spatially Controlled*
429 *Atomic Layer Deposition in Porous Materials*, Applied Physics Lett. 91
430 (2007) 24.
- 431 [22] There are additional effects that make the focusing not exact- see, for ex-
432 ample, A.S. Tremsin, J.V. Vallerga, O.H.W. Siegmund, *Image translational*
433 *shifts in microchannel plate detectors due to the presence of MCP channel*
434 *bias*, Nucl. Instrum. Methods A 477 (2002) 262; A.S. Tremsin, O.H.W.
435 Siegmund, *Spatial distribution of electron cloud footprints from microchan-*
436 *nel plates: measurements and modeling*, Review of Scientific Instruments,
437 70 (1999) pp.3282-3288.
- 438 [23] The measured transverse resolution for the 229-mm 30-strip anode excited
439 by pulses from the microchannel plate detector is 0.5 mm, comparable to
440 the longitudinal resolution of approximately 0.4 mm; detailed studies of the
441 assembled micro-channel plate detector will be presented elsewhere [38]. We
442 note that in applications such as a collider detector, the unique capability of
443 a system of MCP-PMT's is for psec-level time-of-flight. Much more precise
444 spatial measurements are provided by the central tracking systems, but
445 with much poorer timing.
- 446 [24] J.-F. Genat, *Development of a Sampling ASIC for Fast Detector Signals*,
447 Workshop on Fast Timing, Cracow Poland, Nov. 2010.
- 448 [25] M. Wetstein, B. Adams, A. Elagin, R. Obaid, et al., the LAPPD Collabo-
449 ration, in preparation.

- 450 [26] B. Joly, Optimisation de la résolution temporelle en tomographie par
451 émission de positons dédiée au contrôle de dose en hadronthérapie;
452 Ph.D Thesis, Université Clermont Ferrand II- Blaise Pascal, Feb. 2010.
453 <http://tel.archives-ouvertes.fr/docs/00/50/51/29/PDF/BJoly.pdf>
- 454 [27] E. Oberla, *A Fast Waveform-Digitizing ASIC-based DAQ for a Position*
455 *& Time Sensing Large-Area Photo-Detector System*; Photodet2012, LAL
456 Orsay, France; June, 2012.
- 457 [28] http://psec.uchicago.edu/glass/borofloat_33_e.pdf#page=28; The dielec-
458 tric constant is 4.6 and the loss tangent is 37×10^{-4} , both measured at
459 25C and 1 MHz.
- 460 [29] Ferro Corp., 251 Wylie Ave., Washington PA 15301.
- 461 [30] Cat-I Glass, P.O. Box 208, S. Elgin, IL 60177.
- 462 [31] E. Oberla, *A 4-Channel Fast Waveform Sampling ASIC in 130 nm CMOS*,
463 TIPP 2011, Chicago, IL., July 2011, Proceedings to be published in Physics
464 Procedia (Elsevier), 2012.
- 465 [32] The adding or subtracting of a few-millimeter triangle of copper measurably
466 changes the capacitance and inductance at an interface, and is easily seen
467 with the network analyzer.
- 468 [33] Agilent Model HP8753E (6 GHz bandwidth) with Option 010 (time domain
469 option).
- 470 [34] I. J. Bahl and D. K. Trivedi, "A Designer's Guide to Microstrip Line",
471 *Microwaves* (May 1977) 174-182.
- 472 [35] For an excellent discussion of transmission lines, see E. Bogatin, *Signal*
473 *Integrity Simplified*, Prentice Hall Professional Technical Reference, 2004.
474 Chapter 10 is especially clear on cross-talk in striplines.
- 475 [36] R. Harrington, *Time Harmonic Electromagnetic Fields*, IEEE Press (1961).

- 476 [37] R. Brown; Lines, Waves, and Antennas; John Wiley New York.
- 477 [38] M. Wetstein, B. Adams, A. Elagin, J. Elam, H. Frisch, Z. Insepov, V.
478 Ivanov, S. Jokela, A. Mane, R. Obaid, I. Veryovkin, A. Vostrikov, R. Wag-
479 ner Alexander Zinovev et al., to be submitted to Nucl. Instrum. Methods
480 A.

Dr. William A. Barletta
Editor
Nuclear Inst. and Methods in Physics Research, A
In re: Ms. Ref. No.: NIMA-D-12-00776
Title: RF Strip-Line Anodes for Psec Large-Area MCP-based Photodetectors
Nuclear Inst. and Methods in Physics Research, A

Dear Dr. Barletta,

We have resubmitted the above paper with the requested corrections, as detailed below. We'd like to thank the referee for a thoughtful and helpful set of comments. The paper is significantly improved due to the suggestions.

Sincerely, Henry Frisch

Reviewer #1: Dear Authors,

Your paper is very well written and presents a nice, comprehensive set of measurements on your novel strip-line system in a clear manner.

We are grateful for the nice comments.

Overall the paper is maybe a bit longer than required to convey all the information. In particular there seemed to be many instances where text is repeat more than once - sometimes in spirit and sometimes verbatim.

Yes- we have gone through and tightened it in a number of places, removing repetitions. We thank the reviewer for pushing us on this.

Some comments: page 4, line 74/75: I know you are addressing the need for inexpensive systems capable of cover large areas. However, 10's of m² would need 1000s of your tiles, and so calling this a smaller-area application is a little confusing.

Yes- this is now fixed.

p 6, L 115-119: This text is exactly replicated in the caption for Figure 2. Perhaps you could delete one set or use the space to provide different details.

Done.

Fig. 2: Some of the text is very small and difficult to read.

We have remade the figure to be more readable.

Fig. 4: Would it be possible to crop the left hand image and so allow more detail to be visible?

Yes- we have cropped and swapped around the images in Figures 3 and 4 to be much more readable.

Fig. 5: Similar to Fig. 4 in that much of the image is not informative and it is difficult to see the details of the copper tape used for tuning.

We have cropped these so that the details are much more visible.

P 12 L 257 'Launcher' doesn't seem to add any information and appears to be jargon.

Fixed (deleted).

P 15 L 298: same with 'frugal'. Or please define 'frugal' earlier in the paper.

Fixed (deleted).

Figure 10 is a little confusing. Specifically the graph illustrating the pulses on the neighboring strip. Can this be presented more clearly and the various pulses labeled in an enlarged image?

We have remade the figure from scratch, and added a much better caption (thanks!).

Figure 11: The strip numbering schemes in the left and right side images are different. Please make them agree

Yes- now fixed.

Many thanks again to the reviewer. Henry

=====